Orientational Dynamics of Transient Molecules Measured by Nonequilibrium Two-Dimensional Infrared Spectroscopy

Carlos R. Baiz, Robert McCanne, Matthew J. Nee, and Kevin J. Kubarych*

Department of Chemistry, 930 North University Avenue, University of Michigan, Ann Arbor, Michigan 48109

Received: March 26, 2009; Revised Manuscript Received: May 15, 2009

Transient two-dimensional infrared (2DIR) spectroscopy is applied to the photodissociation of $Mn_2(CO)_{10}$ to 2 $Mn(CO)_5$ in cyclohexane solution. By varying both the time delay between the 400 nm phototrigger and the 2DIR probe as well as the waiting time in the 2DIR pulse sequence, we directly determine the orientational relaxation of the vibrationally hot photoproduct. The orientational relaxation slows as the photoproduct cools, providing a measure of the transient temperature decay time of 70 ± 16 ps. We compare the experimental results with molecular dynamics simulations and find near quantitative agreement for equilibrium orientational diffusion time constants but only qualitative agreement for nonequilibrium thermal relaxation. The simulation also shows that the experiment probes an unusual regime of thermal excitation, where the solute is heated while the solvent remains essentially at room temperature.

Introduction

Two-dimensional infrared (2DIR) spectroscopy enables the observation of molecular dynamics such as vibrational energy transfer, spectral diffusion, or ultrafast chemical exchange by using the system's vibrational modes as local probes of molecular microensembles.[1,2] 2DIR also provides time-resolved structural information by measuring the normal mode anharmonicities and couplings, which are directly linked to the underlying vibrational Hamiltonian. Recently, nonequilibrium variants of 2DIR, where the system is optically perturbed before or during the measurement, have been used to investigate phototriggered reactions including metal-to-ligand charge transfer,[3] disulfide bond breaking,[4] and metal−metal bond photodissociation reactions.[5,6]

These two-dimensional experiments build upon more traditional techniques such as one-dimensional pump−probe measurements, which continue to successfully reveal new information on the dynamics of chemical systems under nonequilibrium conditions. For example, the mechanisms for reorientational dynamics and resonant energy transfer in liquid water have been revealed by polarization-resolved infrared pump−probe spectroscopy.[7,8] Similar experiments have investigated the orientational dynamics of carbon monoxide following photodissociation from a heme host in hemoglobin[9] and myoglobin.[10] It was found that, upon dissociation, the ligand finds specific docking sites within the heme pocket where it remains for several nanoseconds, suggesting the existence of an energy barrier for the recombination process. Recently, these results were further expanded upon by mapping the photoinduced ligand migration to the docking sites and the subsequent interconversion between the distinct conformations in myoglobin by triggered-exchange 2DIR spectroscopy.[11] In the present Article, we measure the orientational dynamics of a transient radical species via transient 2DIR spectroscopy. It is important to emphasize the key difference between the molecular information provided by transient-2DIR in comparison to established one-dimensional anisotropy measurements: A typical UV-pump/IR-probe anisotropy experiment, such as the one described above, reports on the orientational correlation of the transition dipole moment of a photoproduct IR transition with respect to the excited electronic transition dipole moment of the initial state. The orientational information contained in transient-2DIR reports on the self-correlation of the photoproduct species at different delays following photodissociation. For sufficiently long delays between the photolysis pulse and the 2DIR probe, there is no correlation at all between the photodissociation and the photoproduct transition dipole moments. Thus, this new technique probes the changing dynamics of the transient species itself en route to thermodynamic equilibrium.

Nonequilibrium classical dynamics simulations have been successful in modeling solute to solvent vibrational energy relaxation in multiple systems, and the theory of classical and semiclassical energy relaxation is well-established within this context.[12−16] In a recent paper, Backus and co-workers[17] used nonequilibrium molecular dynamics (MD) simulations to model vibrational energy transport among isotope-labeled carbonyl modes in a short peptide. Carbonyl vibrations were excited either directly in the IR or by UV excitation of an azobenzene chromophore attached to one of the peptide's termini where the excess electronic energy subsequently relaxes into the vibrational modes. Although transient absorption results show that the rate of transport is slower when exciting the chromophore, the rate obtained from MD simulations is insensitive to the type of excitation. The MD results agreed well with the low-energy excitation experiments, but yielded rates that were too fast in the case of UV excitation.

Metal Carbonyls. The photochemistry of $Mn_2(CO)_{10}$ has been the focus of numerous studies mainly aimed at understanding the excited-state reaction pathways and subsequent energy relaxation processes.[18−31] Two dissociation pathways have been demonstrated: excitation at 400 nm primarily cleaves the Mn−Mn bond, producing 2 $^{\bullet}Mn(CO)_5$ radicals, whereas excitation at 342 nm dissociates one carbonyl ligand to yield $Mn_2(CO)_9$.[25,29] In both cases, the bond energy is substantially less than the excitation energy, causing the products to remain in a vibrationally hot state after photodissociation.

Steinhurst et al.[29] measured the 1982 cm^{-1} absorption line shape narrowing of $Mn(CO)_5$ photoproducts with excitation at

* Corresponding author. E-mail: kubarych@umich.edu.

10.1021/jp9027595 CCC: $40.75
Published on Web 06/12/2009

400 nm using time-resolved infrared spectroscopy and found the narrowing lifetime in cyclohexane to be 44.7 ± 17.4 ps. The results also showed that the narrowing lifetime is shorter in polar solvents due to stronger solute−solvent interactions, an effect also observed in photodissociation of other metal carbonyls.[18] Although a detailed discussion of temperature-dependent absorption line widths was not presented, the authors concluded that this narrowing lifetime provided a lower limit for the vibrational cooling of the product molecules as they did not observe any contribution to the absorption from anharmonic transitions. Other related studies have reported similar rates for low frequency mode relaxation in similar metal carbonyls.[18,32,33] The UV-pump/visible-probe measurements of Zhang et al.[31] found the relaxation of $Mn(CO)_5$ following photolysis at 295 nm to exhibit biexponential behavior with a ~15 ps fast component and a ~180 ps slow decay. The authors attributed the fast component to intramolecular vibrational relaxation of the CO modes through low frequency modes of the molecule, and the slow component was ascribed to ultimate relaxation to the solvent. Although these previous studies have provided significant insight into the photochemistry of $Mn_2(CO)_{10}$, a full understanding requires the characterization of excited-state lifetimes and quantum yields, as well as geminate rebinding rates and mechanisms.

In this Article, we report our measurements of orientational relaxation rates of $Mn(CO)_5$ as a function of the time delay after photodissociation as obtained by transient-2DIR spectroscopy. The response function underlying the 2DIR spectrum includes the same orientational dynamics typically probed using absorption anisotropy, and due to the separation of time scales, we are able to extract the orientational component of the transient 2DIR spectra. We use the measured orientational lifetimes to determine the system-solvent energy dissipation rate (cooling) after photodissociation. These experiments create conditions unique to nonequilibrium phenomena where, due to weak solute−solvent coupling, the temperature of the solute increases following photodissociation while the solvation shell remains at nearly a constant temperature. Orientational relaxation rates are used as a molecular thermometer, which indirectly report on the excitation of the low-frequency modes. Similar ultrafast methods, such as IR−Raman spectroscopy, have also been useful in providing mode-specific populations in various nonequilibrium systems.[34−36] To further elucidate the dynamics of $Mn(CO)_5$ transient species, classical dynamics simulations are used in modeling temperature relaxation and orientational lifetimes. In addition, temperature dependence of transient-absorption line shape is modeled using an anharmonic description based on vibrational perturbation theory.

Orientational Diffusion. The rate of orientational relaxation is commonly written in the context of Debye−Stokes−Einstein theory. Within this framework, the orientational correlation time is expressed in terms of the solvent viscosity η, the specific volume of the molecules v_s, and the temperature (T) as

$$\tau_R = \frac{C\eta v}{k_B T} \tag{1}$$

where k_B is Boltzmann's constant, and C is an empirical constant. If the transition dipoles are assumed to be invariant with respect to the bath degrees of freedom, as in the Condon limit, the molecular reorientational time can be approximated as the dipole−dipole correlation time of a single vibrational transition, as the angle between the transition dipoles and the molecular axis are invariant with time. It is important to note the inverse temperature dependence of the correlation function; below we provide a discussion of measured temperature-dependent orientational dynamics, and, using this relationship, we extract the cooling rate of the transient $Mn(CO)_5$ species following photoexcitation.

It is well-known that the infrared pump−probe anisotropy $r(t)$ for an individual vibrational transition can be written as a function of the dipole−dipole time correlation function.[37,38]

$$r(t) = \frac{I_{||}(t) - I_{\perp}(t)}{I_{||}(t) + 2I_{\perp}(t)} \tag{2}$$

In the above equation, $I_{||}(t)$ and $I_{\perp}(t)$ represent the pump−probe intensity measured with parallel and perpendicular relative polarizations. These two contributions can also be written as

$$\begin{aligned} I_{||}(t) &= \left[\frac{1}{3} + \frac{4}{15}C_2(t)\right]P(t) \\ I_{\perp}(t) &= \left[\frac{1}{3} - \frac{2}{15}C_2(t)\right]P(t) \end{aligned} \tag{3}$$

where $P(t)$ is the population of the excited state, and $C_2(t)$ is the second Legendre polynomial of the dipole−dipole time correlation function averaged over all of the initial configurations. The orientational contribution to the anisotropy decay, obtained by combining eqs 2 and 3, is written in terms of the dipole−dipole correlation function as:

$$\begin{aligned} r(t) &= \frac{2}{5}C_2(t) \\ C_2(t) &= \langle P_2[\vec{\mu}(0)\cdot\vec{\mu}(t)]\rangle \end{aligned} \tag{4}$$

The orientational contribution to the 2DIR signal in the *zzzz*-polarization geometry is similarly expressed as a function dipole−dipole correlation function:[39]

$$Y_{zzzz}(t_1, t_2, t_3) = \frac{1}{9}\left([C_1(t_1)C_1(t_3)]\left[1 + \frac{4}{5}C_2(t_2)\right]\right) \tag{5}$$

From the above relation, we observe that the orientational contribution to the waiting time-dependence of the 2D signal is the same as for the one-dimensional anisotropy. The orientational equations for transient-2DIR spectroscopy, a fifth-order experiment, are significantly more complex as the UV pulse preselects a subensemble of the molecules.[40,41] However, in our experiments, the time between the UV and IR pulses is at least 40 ps, and because the orientational lifetime of the photoproducts is ~10 ps (see below), the 2DIR experiment is essentially done on an isotropic ensemble. This clear separation of time scales allows us to apply the simpler third-order version of the orientational equations outlined above.

Ultrafast Measurements and Modeling Methods

Experimental Setup. The nonequilibrium time-domain 2DIR spectrometer has been described in detail elsewhere.[42] Briefly, mid-infrared pulses (2 μJ, 100 fs), centered at 2000 cm^{-1} with ~100 cm^{-1} fwhm bandwidth, are generated using a dual-optical parametric amplifier/difference frequency generation setup pumped by a regeneratively amplified Ti:Sapphire laser. The mid-IR pulses are split into k_1, k_2, k_3, tracer, and reference beams. The UV pulses (>30 μJ, ~100 fs) are obtained by frequency-

doubling ~200 μJ of the laser output in a 0.4 mm BBO crystal and stretched to ~400 fs using a 10 cm fused silica block to minimize multiphoton interactions with the sample. An interferometrically stable wire-guided jet[43] is used to refresh the sample volume between laser shots. The UV beam is mechanically chopped with a 50% duty cycle synchronized to the 1 kHz amplifier repetition frequency. To collect a transient 2DIR spectrum, the delay of the first IR pulse (k_1) is scanned continuously, and the heterodyned rephasing signal is upconverted into the visible using a highly chirped pulse (fwhm = 160 ps) centered at 800 nm[44] and detected at the laser repetition rate in a spectrometer using a silicon-based CCD detector. The collected time-domain data are deinterlaced into separate interferograms corresponding to pumped (UV on) and unpumped (UV off) and are processed separately. The final difference 2D spectrum is computed in the frequency domain by subtracting the unpumped from the pumped absolute value rephasing spectra. To measure the photoproduct relaxation rates, we collected transient-2DIR spectra at different t_2 delay times, between 0 and 20 ps using 50 steps spaced such that the relaxation is more densely sampled at the beginning of the exponential decay. These experiments were repeated at six different UV−IR time delays ranging from 40 to 300 ps; 120 transient-2DIR spectra were collected in total. Errors arising from laser drift and long-time instabilities of the liquid jet were minimized by randomizing the order in which the spectra were acquired.

UV-pump/IR-probe spectra were collected by measuring the differential transmission of the tracer pulse while chopping the UV and IR pump pulses, respectively, and blocking all of the other beams. Equilibrium IR-pump/IR-probe measurements used to obtain anisotropy decays of the parent molecules were collected by recording the differential probe transmission at two polarization configurations while chopping k_1 and blocking all of the other beams. Similarly, transient-pump−probe spectra were obtained by combining the UV and IR pump beams, chopping the UV at 500 Hz and the IR at 250 Hz, and recording the tracer transmission at the laser repetition frequency of 1 kHz. Experimental pulse sequences are shown in Figure 1. $Mn_2(CO)_{10}$ solutions (6 mM) were prepared using spectrophotometric grade cyclohexane. This concentration produces an optical density of ~0.30 at the $Mn_2(CO)_{10}$ main absorption peak (2013 cm^{-1}) with a ~200 μm path length in the liquid jet. All chemicals were purchased from Sigma-Aldrich and were used without further purification.

Nonequilibrium Molecular Dynamic Simulations. The cyclohexane solvent was modeled using the all-atom general AMBER force field,[45,46] and atomic charges were assigned ab initio using the restrained electrostatic potential (RESP) scheme[47,48] computed with Gaussian 03.[49] The metal carbonyl force fields were parametrized using harmonic potentials and Mulliken atomic charges derived from density functional theory (DFT) with B3LYP/6-31+G(d). One molecule of $Mn_2(CO)_{10}$ was placed in a cubic box containing 507 solvent molecules. The system was energy-minimized and equilibrated for 1 ns with 1 fs integration steps at 298 K and 1 bar using a Berendsen thermostat.[50] The simulations were performed using the leapfrog algorithm as implemented in GROMACS, long-range electrostatic interactions were treated using the particle-mesh Ewald method, the nonbonded neighbor lists were updated every 10 integration steps, and the interaction cutoff was set to 1.0 nm. After equilibration, a 2 ns $Mn_2(CO)_{10}$ production trajectory was generated under the same simulation conditions. The same procedure was used to generate a 2 ns equilibrium trajectory

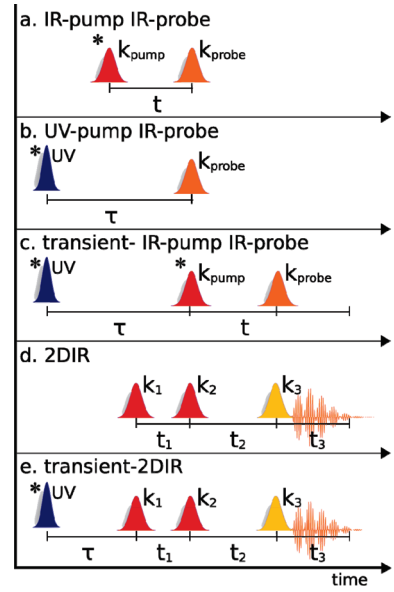

Figure 1. Pulse sequences corresponding to the various experiments described throughout this Article. The blue pulse represents the UV phototrigger pulse, the red pulses represent IR pump pulses, k_1 and k_2, in 2DIR experiments, orange corresponds to the tracer pulse, used in one-dimensional pump−probe experiments, and the yellow pulses correspond to k_3 used in the two-dimensional experiments. The pulses marked with a star are mechanically chopped during the experiment.

for $Mn(CO)_5$. From the 2 ns trajectory for $Mn(CO)_5$, 50 independent conformations were obtained as starting points for the nonequilibrium simulations. The quantum description of vibrational energy redistribution is quite complex. For example, the energy distribution ratios among the modes could be obtained by propagating the full quantum anharmonic Hamiltonian. However, because the simulations are classical in nature, and thus would not be able to accurately capture the effects of vibrational energy transfer,[17] it would be of questionable utility to compute the full quantum mechanical energy distribution ratios as an input to the classical simulations. As an approximation, the photolysis reaction and subsequent energy redistribution were simulated by scaling the velocities of all of the atoms in $Mn(CO)_5$ to account for the excess energy that remains after dissociation. At each starting conformation, the equilibrium kinetic energy was computed, and all of the atomic velocities in $Mn(CO)_5$ were scaled by a factor that yielded a final kinetic energy equal to the equilibrium energy plus excess excitation energy: The Mn−Mn bond energy is estimated to be 12 600 cm^{-1},[20] which leaves 12 400 cm^{-1} of excess energy after photodissociation with 400 nm excitation. Using the DFT-derived heat capacity, the temperature of $Mn(CO)_5$ immediately following photodissociation is predicted to be 664 K. The nonequilibrium NVE trajectories were run for 100 ps using integration steps of 0.2 fs, and atom positions and velocities were collected every 10 fs for analysis. From these trajectories, the temperature of the molecule and the solvation shell (nearby cyclohexane molecules) were computed. Dipole−dipole time correlation functions for the parent molecules and photoproducts were also computed from the 2 ns equilibrium simulations. All simulations were performed using the GROMACS 3.3 package of programs.[51]

Theoretical Line Shapes. To simulate the temperature-dependent absorption line width of $Mn(CO)_5$, we employ an anharmonic description based on a previous model by Hamm et al.,[52] which accounts for the thermal excitation of low-frequency (bath) modes and their effect on the frequency of

the CO stretch mode of interest. We begin by computing a set of third- and semidiagonal fourth-order anharmonic force constants for all of the modes using standard electronic structure methods (B3LYP, LANL2DZ on Mn, 6-31G(d) on C and O), as described in the Supporting Information. These anharmonic force constants are obtained by displacing the molecular geometry along the normal modes and computing the change in harmonic frequencies between the equilibrium and displaced geometries.[53,54] The anharmonic coupling constants, X_{ii} and X_{ik}, which represent the shift in frequency of mode k given that mode i is excited, are computed using second-order vibrational perturbation theory (VPT2). The computation of anharmonic coupling constants from electronic structure methods via VPT2 is well-established, and the procedure is described in detail elsewhere.[55,56] It is important to note that the described DFT/VPT2 procedure successfully reproduces the experimentally measured carbonyl anharmonicities in $Mn_2(CO)_{10}$, therefore justifying its use in this work.[57] A temperature-dependent absorption line shape $A_k(\omega)$ of the carbonyl stretching mode of interest k is written as:

$$A_k(\omega) = \upsilon_k + \sum_{i \neq k} \sum_{n_i} Q^{-1} \exp(-n_i \upsilon_i / kT) \exp(-[\omega - \upsilon_k - n_i X_{ik}]^2/\sigma^2) \quad (6)$$

The first exponential inside the sum represents the thermal probability that a bath mode i will be in the nth excited state at temperature T with a normalization factor $Q(T)$; the second term is a Gaussian function centered at a frequency shifted from the fundamental by $n_i X_{ik}$. In the above equation, υ_i represents the fundamental transition of mode i in the anharmonic description, computed by:

$$\upsilon_k = \omega_k + 2X_{kk} + \frac{1}{2}\sum_i X_{ik} \quad (7)$$

where ω_k is the harmonic frequency of mode k, and X_{kk} and X_{ik} are the anharmonic coupling constants described above. A full set of coupling constants along with the harmonic and anharmonic frequencies for $Mn(CO)_5$ is given in the Supporting Information. It is important to note that in our model the high frequency mode k remains in the ground state, an approximation that only applies to systems where the mode of interest has negligible thermal population. In the above expression for $A_k(\omega)$, the first summation is over all of the bath modes; in our case, we define the bath modes as all of the normal modes with frequencies lower than the lowest frequency terminal CO stretch. We explicitly exclude the solvent degrees of freedom due to the very weak coupling, manifested in the long vibrational lifetime. The second summation in eq 6 is over all excitations of these modes; from a practical perspective, we found that including 10 excitations is sufficient to converge the results at a temperature of 600 K or below.

Results

Equilibrium Anisotropy. Equilibrium IR-pump/IR-probe anisotropy measurements, shown in Figure 2, report directly on the orientational relaxation lifetime of the parent molecule, $Mn_2(CO)_{10}$. The transient absorption anisotropy shown for the central 2013 cm^{-1} band exhibits biexponential behavior with a fast component of ~600 fs caused by rapid randomization of energy among the carbonyl modes (IVR), and a slower component due to the orientational relaxation. The initial value of 0.2 is consistent with the fact that the 2013 cm^{-1} band is due to two doubly degenerate modes with perpendicular transition moments.[44] This measured relaxation lifetime of 15.8 ± 3.5 ps can be directly compared to the calculated MD lifetimes as shown below.

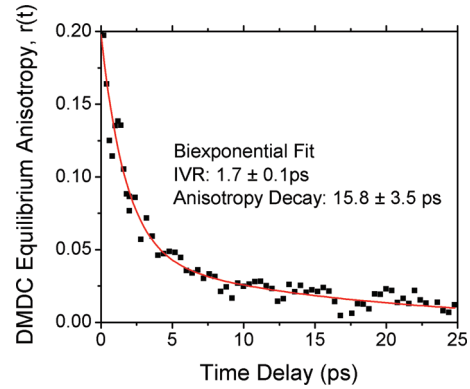

Figure 2. $Mn_2(CO)_{10}$ equilibrium anisotropy obtained by measuring IR-pump/IR-probe differential absorption of the 2013 cm^{-1} transition in the parallel and perpendicular polarization geometries. The initial fast decay is due to IVR, and the slower decay represents the orientational relaxation of the equilibrium species. The initial value of 0.2 is attributed to the fact that the probed frequency corresponds to two degenerate CO stretching modes with perpendicular transition dipole moments.

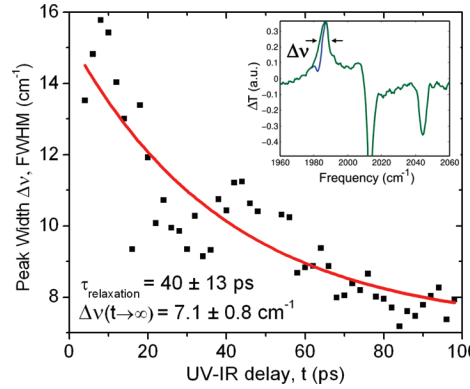

Figure 3. Transient peak widths obtained from one-dimensional UV-pump/IR-probe transient absorption experiments with a single-exponential fit. The inset shows the transient absorption spectrum at long UV−IR delay (100 ps) after bleach subtraction. The green and blue curves represent the transient absorption before and after bleach subtraction near 1982 cm^{-1}, respectively (see text for details).

UV-Pump/IR-Probe. The broad bandwidth of the induced photoproduct absorption observed in the one-dimensional UV-IR transient spectra has previously been attributed to the population of low-frequency modes (heating) in the photoproduct by the excess energy remaining after photodissociation. To obtain a system-to-solvent energy transfer lifetime (cooling), we measure the absorption line width in UV/IR transient absorption spectra collected from 10 to 100 ps delay at 2 ps steps as shown in Figure 3. The overlapping bleach is removed by fitting the 1982 cm^{-1} feature in a single long-delay pump−probe spectrum to two Gaussian functions, one positive and one negative, and then subtracting the negative Gaussian from all of the other pump−probe spectra. After the bleach was removed in each spectrum, the photoproduct transient peak centered near 1982 cm^{-1} is fit to a single Gaussian function. The full-width-at-half-maximums of the Gaussian fits are plotted (Figure 3) as a function of the UV−IR time delay, and the data are fit to a single exponential. This procedure yields a relaxation

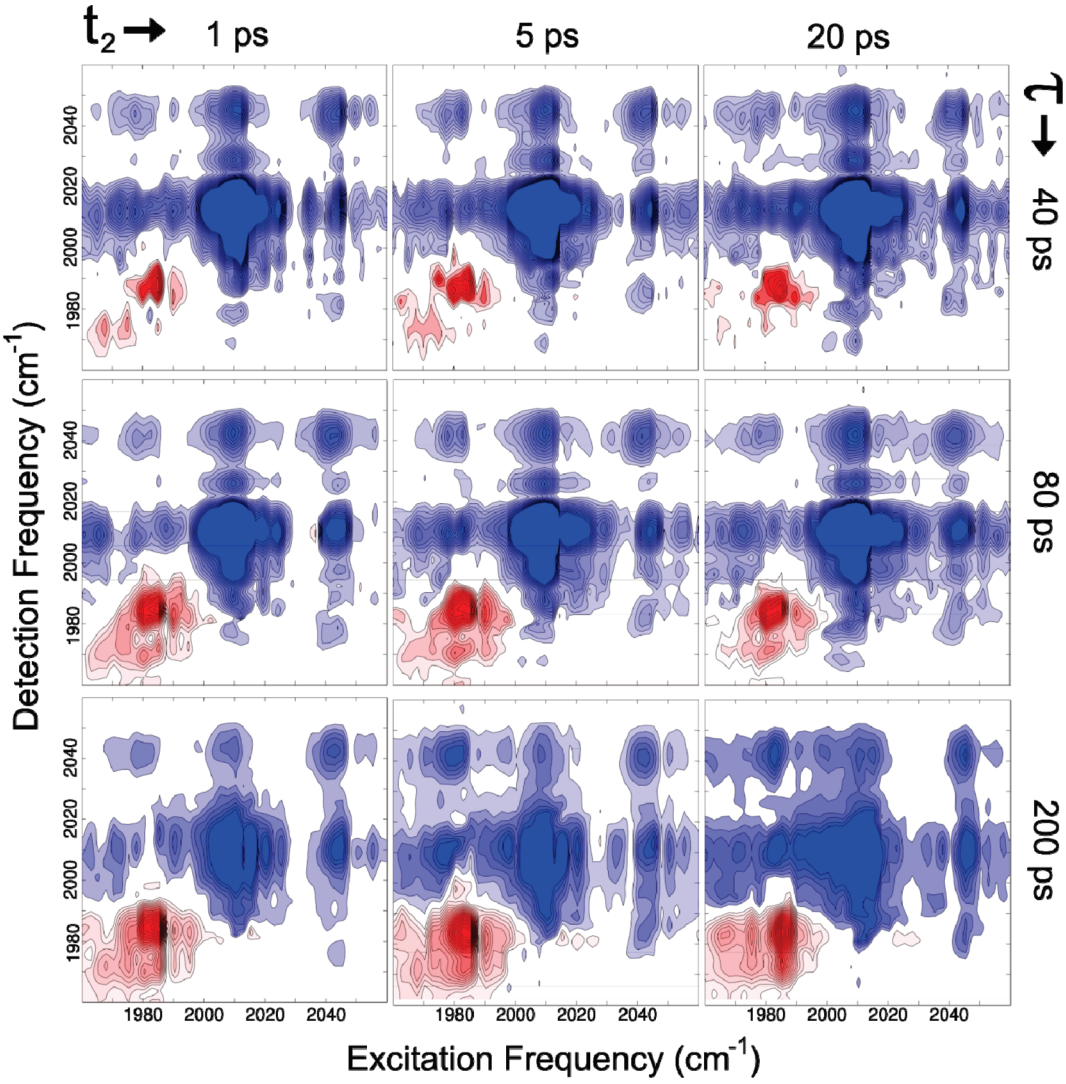

Figure 4. Transient-2DIR spectra of $Mn_2(CO)_{10}$ obtained at different waiting times (t_2) and multiple UV-2DIR delays (τ) [see Figure 1]. The negative features, shown in blue, represent the bleaches corresponding to depletion of parent $Mn_2(CO)_{10}$ molecules, and the red feature (lower left) represents the absorption due to the transient $Mn(CO)_5$ radical species. The transient signal is initially weak and becomes stronger as the photoproduct molecules reach the final equilibrium temperature. Contour spacing is normalized to the maximum signal difference, and contours that are smaller than 2% or larger than 40% of the total bleach amplitude are removed for clarity.

lifetime of $Mn(CO)_5$ in cyclohexane of 40 ± 13 ps, which is in excellent agreement with the previously published lifetime of 44 ± 17 ps.[29] The data also show that the line width remains broad at long UV−IR time delays (see discussion below). Additionally, the $Mn_2(CO)_{10}$ bleaches do not recover within the time scale of the experiment (200 ps). Previous experiments[29] also reported an instrument response limited onset of the bleach and the absence of bleach recovery even at 500 ps after photoexcitation; Dougherty et al.[18] reported a bleach recovery in the 5−400 μs regime in $Rh(CO)_2(acac)$, suggesting that nongeminate recombination is a diffusion-limited process.

Transient-2DIR. The equilibrium absolute-value rephasing 2DIR spectrum of $Mn_2(CO)_{10}$, described in detail elsewhere,[44] exhibits nine main peaks, diagonal peaks at 1983, 2013, and 2045 cm^{-1}, and six cross-peaks, which correspond to Liouville paths involving light interactions with different vibrational modes during the infrared excitation and detection times. As the waiting time t_2 is increased, these off-diagonal peaks oscillate at the difference frequency between the corresponding diagonal modes. The transient-2DIR spectra (Figure 4) show bleaches as a result of depletion of parent molecules and a transient peak centered near [$\omega_1 = 1982$, $\omega_3 = 1982$ cm^{-1}] due to the nascent photoproduct molecules. The 2D line shape of this peak is somewhat distorted due to spectral overlap with the low-frequency diagonal bleach. To minimize these distortions, the IR pulses were tuned to the high-frequency region of the spectrum so as to decrease contributions from low-frequency bleaches. Similar to the previously reported 1D transient absorption spectra,[29] this transient 2D peak is initially broad and becomes narrower with increasing UV−IR time delay due in part to vibrational cooling. Three different processes contribute to the signal decay along t_2: intramolecular vibrational redistribution, orientational relaxation, and vibrational relaxation. The different time scales for these three processes allow for clean isolation of the orientational contribution as discussed below. Relaxation rate constants are obtained by integrating the volume of the entire transient 2D peak (red features in Figure 4) for each value of t_2 and fitting the t_2 decay to a single exponential. To reduce the errors arising from the exponential fitting of the relaxation data, the integrated peak volume is low-pass Fourier filtered and is fit starting at $t_2 = 2$ ps to remove the contribution from the rapid initial decay ($\tau \approx 600$ fs), which arises from intramolecular vibrational redistribution. The filtering also removes any errors due to coherent oscillations of the

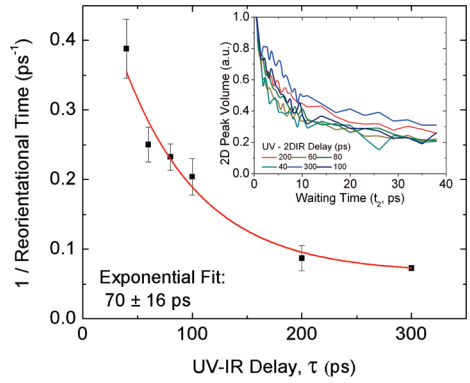

Figure 5. $Mn(CO)_5$ reorientational time constants as a function of the UV-2DIR time delay, τ, obtained from the integrated transient peak volumes as a function of the 2DIR waiting time, t_2. The solid curve is a single-exponential curve fit to the data showing a decay time of 70 ± 16 ps. This exponential represents the cooling of the molecules after photoexcitation. Additional information about the fitting process and a representative fit are provided in the Supporting Information.

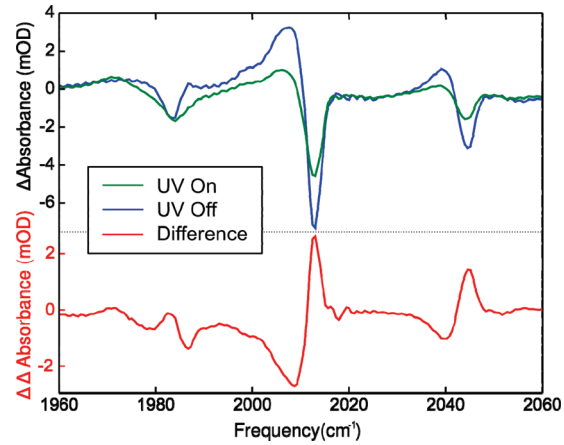

Figure 6. IR-pump/IR-probe spectra obtained with (green) and without (blue) the UV pump. The pumped (UV on) spectrum shows smaller changes at 2045 and 2013 cm^{-1} due to the depletion of parent molecules and shows a comparable bleach intensity at 1982 cm^{-1} because of the absorption of the new transient species generated by the UV phototrigger. The difference (UV on−UV off, red) spectrum clearly shows the increase in signal near 1982 cm^{-1} due to the photoproducts.

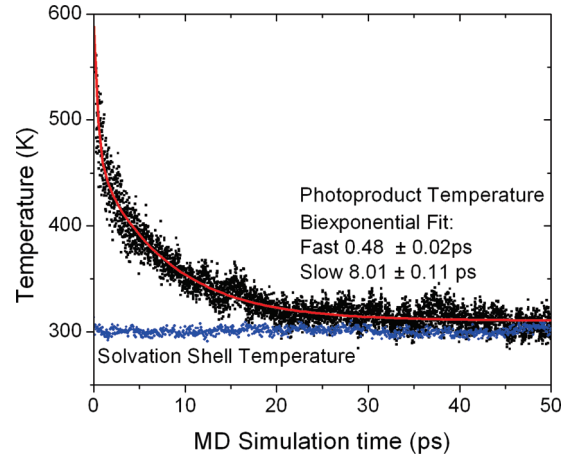

Figure 7. Temperature of the $Mn(CO)_5$ species following photodissociation obtained from the nonequilibrium MD simulations using an average of 50 nonequilibrium trajectories. The temperature of the solvation shell, which remains near the equilibrium value, was obtained by identifying the six nearest cyclohexane molecules at each MD step and computing their average temperature.

overlapping parent peaks observed at small waiting times.[58] Although the decay constants obtained from the curve fitting may still contain errors that arise from vibrational energy relaxation or the fitting procedure itself, we expect these errors to be similar for all of the curves as the same procedure is applied to all of the decay curves. The relative change in the relaxation rates as a function of the UV−IR delay should therefore be reliable. The Debye−Stokes−Einstein relationship makes it possible to obtain an effective temperature decay from the set of orientational relaxation curves. The orientational rate constant (inverse decay time) is directly proportional to the temperature of the system, allowing the direct mapping of the UV−IR time delay axis to a molecular temperature axis. It is important to note that as verified by the simulation study discussed below, in this experiment the temperature and viscosity of the solvent remain at their equilibrium values; the only variable is the temperature of the solute molecules. The relaxation rate constants plotted as a function of the UV−IR delay along with the temperature decay are shown in Figure 5.

Transient UV-Pump/IR-Pump−IR-Probe. The transient UV-pump/IR-pump−IR-probe spectra, shown in Figure 6, can be best understood as two IR-pump/IR-probe spectra with and without the presence of nonequilibrium photoproducts in solution. The negative-going bleaches observed correspond to the depletion of ground vibrational state molecules caused by the IR pump with the corresponding anharmonically shifted increase due to excited-state absorption (ESA). The UV pump causes a depletion of parent molecules and generates photoproduct molecules, which, aside from the induced photoproduct, yield a similar ground-state bleach (GSB) and ESA signal. In the IR/IR experiments, two processes contribute to the GSB signal, the depletion of ground-state molecules and the stimulated emission from the populated excited states. The broad 1982 cm^{-1} peak in the UV-pumped spectrum is caused by the overlapping contributions of both the parent and the daughter species. To remove these contributions, the difference between the two pump−probe spectra is computed. The data show that the ESA of the photoproducts directly overlaps the GSB from the parent molecules. In principle, the same orientational relaxation information contained in the transient-2DIR experiments is present in the transient-pump−probe data (see eq 3); however, spectral overlap between the low-frequency bleach and transient peak along with a low signal-to-noise ratio, due to slow signal drift as the IR/IR delay is scanned, prevented the extraction of reliable orientational relaxation lifetimes from these data. Pump−probe and 2DIR signals arise from the same light-matter interactions and thus contain similar information. One advantage of 2DIR over one-dimensional pump−probe relies on the fact that the 2DIR signal is emitted in a background-free direction, whereas the pump−probe signal is emitted in the same direction as the probe beam. In which case, to avoid saturating the detector, the probe beam must be weak. Because the intensity of the signal is proportional to the intensity of the pump and probe pulses, in the pump−probe experiments the signal is usually weaker, and additional signal averaging is required to obtain reliable data. In addition, comparing the transient-pump−probe and transient-2DIR spectra, it is possible to observe that the photoproduct peak height is larger with respect to the bleaches, and better isolated in the 2DIR data, making the extraction of orientational relaxation rates possible.

MD Simulations. A plot of temperature versus time, as shown in Figure 7, is obtained from the MD simulations, indicating that adding 12 400 cm^{-1} of excess kinetic energy causes an initial temperature of ∼587 K, in reasonable agree-

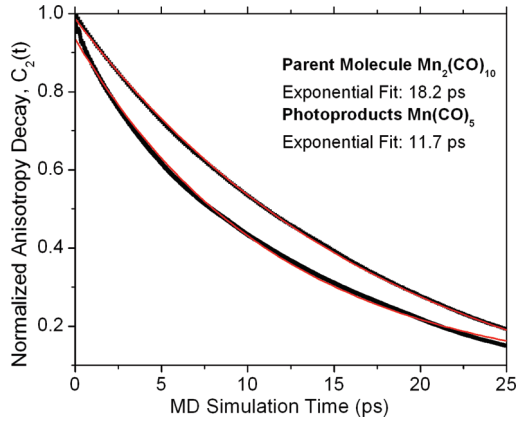

Figure 8. Orientational relaxation contribution to the anisotropy and 2DIR signal decays computed from the MD simulation via the dipole−dipole time correlation (black) function along with their exponential fit (red). The curve corresponding to the photoproduct was obtained from MD data collected from the 2 ns equilibrium (NPT) trajectory.

ment with the result predicted via the DFT-derived heat capacity. It is well-known that the classical heat capacity of a molecule is larger than the quantum heat capacity; thus one would expect the MD simulations to show a smaller increase in temperature than the increase calculated using the DFT heat capacity. The similarity arises because dihedral angles are not specifically parametrized in the classical force field, and thus these low-frequency vibrations, which may have a large contribution to the heat capacity, are not present in the classical simulations. A biexponential curve is needed to accurately fit the temperature data, giving a fast component of ∼480 fs and a slower component of 8.01 ps. The slower component is attributed to energy relaxation to the solvent (cooling). To further elucidate the energy relaxation process, we computed the temperature of the solvation shell and found it to remain constant near the equilibrium value of 298 K, indicating that the heat diffusion within the solvent is an efficient process. In addition, we simulated the photodissociation reaction by simply removing the Mn−Mn bond from the force field and scaling the velocities of the atoms but observed that the two $Mn(CO)_5$ molecules formed stable dimers in every computed nonequilibrium trajectory. The temperature decay time of the dimers (8.94 ps) is similar to that of the monomers, suggesting that the molecule−solvent interactions remain mostly unaffected.

Simulated Equilibrium Orientational Relaxation. Orientational relaxation curves were obtained from the equilibrium and nonequilibrium trajectories by fixing the molecular axis along one of the equatorial carbonyl bonds and computing a time autocorrelation of the vector dot product trajectory. The second Legendre polynomial of this autocorrelation function is directly proportional to the orientational contribution to the anisotropy, as well as the 2DIR waiting-time decays as noted in eqs 4 and 5. Orientational relaxation curves for the parent molecule obtained from the MD simulations (Figure 8) show single exponential behavior with a lifetime of 18.2 ps. The photoproduct exhibits a biexponential relaxation that is likely due to the two $Mn(CO)_5$ dimer structures. However, the two exponentials have nearly equal amplitude, and the decay curve is adequately fit with a single exponential, allowing direct comparison with the 2DIR experimental decay curves. The temperature dependence of the orientational relaxation constants was not computed from the simulations because, to achieve this, either the entire simulation box would need to be heated to a higher temperature or the solute and solvent would have to be simulated under different thermostats, neither of which reproduces the experimental conditions.

TABLE 1: Summary of the Orientational Relaxation Constants Obtained from Experiment and from the Molecular Dynamics (MD) Simulations

method	orientational relaxation (ps)	cooling rate (ps)	species
equilibrium anisotropy	15.8 ± 3.5		$Mn_2(CO)_{10}$
UV-pump/IR-probe		44 ± 17 (lower limit)	$Mn(CO)_5$
transient-2DIR	13.7 ± 0.7 (τ = 300 ps)	70 ± 16	$Mn(CO)_5$
equilibrium MD	18.2		$Mn_2(CO)_{10}$
equilibrium MD	11.7		$Mn(CO)_5$
nonequilibrium MD		8.0	$Mn(CO)_5$

Discussion

Orientational Relaxation. Table 1 summarizes the orientational relaxation and cooling rates obtained from experiment and MD simulations. The 2DIR signal decay along the waiting time is characterized by three main contributions with substantially distinct time scales: intramolecular vibrational relaxation (∼1 ps), orientational diffusion[59] (∼5−10 ps), and vibrational energy relaxation to the solvent (∼100 ps). The separation of these time scales enables isolation of the orientational contribution to the transient 2DIR signal by fitting the overall signal decays as described above. The decay times range from 2.5 to 12 ps, consistent with the transient IR-pump/IR-probe anisotropy measurements of the parent molecules, where we observe a similar reorientation time scale showing that these decays are indeed due to orientational dynamics.

The key experimental observation of this work is that the orientational relaxation times are dependent on the UV-2DIR waiting time. It is a unique feature of the additional temporal and spectral correlation made possible by nonlinear 2D spectroscopy that reorientation of a transient species can be directly observed in the time domain. Previous experiments have suggested that initial molecular reorganization of metal carbonyl photoproducts likely occurs on an ultrafast time scale.[30] Therefore, by the time of our first 2DIR measurement (40 ps), the molecules should be largely at equilibrium in this regard. It is also known, from the long CO vibrational lifetimes (∼100 ps) and narrow infrared transitions observed in metal carbonyls in nonpolar solvents (3−5 cm^{-1} in $Mn_2(CO)_{10}$), that the system−solvent interactions are weak, and thus the molecules are largely isolated from the solvent. Therefore, it is expected that the process of heat transfer between the molecule and the solvent should be slow with a time scale comparable to that of vibrational energy relaxation.

The observed evolution in the orientational relaxation as the UV-2DIR delay is then due to temperature effects. Orientational diffusion occurs faster when the molecules are in a hot state and slower as the molecules reach the final equilibrium temperature. Because of weak system−solvent interactions, the solvent remains at a constant temperature, as indicated by the molecular dynamics simulations, and therefore the viscosity of the liquid is properly regarded as remaining constant. This scenario is in contrast to other ultrafast temperature-dependent relaxation experiments where the solvent and solute are in thermal equilibrium; thus solvent viscosity changes and changes in the material density can significantly influence the measurements and should be explicitly included in the data analysis.[60,61]

To further elucidate the effects of orientational relaxation on the 2DIR waiting-time signal decay, we analyze the results

obtained from molecular dynamics simulations. The simulated photoproduct orientational decay of 13.4 ps is in excellent agreement with the experimental values at long time delays of 11.7 ps. In the equilibrium case, the simulations predict a slightly longer decay time of 18.2 ps, which is also in agreement with the experimental value of 15.8 ps measured in the anisotropy experiment (Figure 2). Although such good agreement is likely a coincidence as we do not expect the MD simulations to quantitatively reproduce the experimental values, the experimental trend is clearly captured in the simulation. The similarity in relaxation rates for the $Mn_2(CO)_{10}$ and $Mn(CO)_5$ molecules arises from the similar forces experienced by both species in the simulations. It is also observed that the $Mn(CO)_5$ orientational decay is biexponential in nature (Figure 8), an effect attributed to the fact that $Mn(CO)_5$ is a symmetric top. The decay is, nonetheless, adequately fit with a single exponential function, and it is unlikely that this behavior would be observed experimentally, as an extremely high signal-to-noise ratio would be required.

On the basis of the observed changes in orientational lifetime as a function of UV-2DIR time delay, we are now in a position to apply Debye−Stokes−Einstein (DSE) theory and directly correlate the differences in orientational relaxation rates to the temperature of the molecule. The main underlying assumption that allows us to obtain a cooling rate from DSE theory is that the molecular degrees of freedom of the solute are completely equilibrated; the energy is partitioned among all of the degrees of freedom, and a single temperature can be used to describe the system. This is a reasonable assumption because it is likely that collisions with the solvent would rapidly partition the energy among all degrees of freedom in the system, particularly given that the 2DIR measurements are preformed starting at 40 ps after the photoreaction. The understanding of these temperature-dependent orientational relaxation rates is rather intuitive; part of the excess excitation energy is channeled into the low-frequency vibrational and rotational modes of the molecule, causing an increase in the collision rate with the solvent and thus increasing the rate of orientational diffusion. Next, we discuss the cooling rates based on the evidence from one-dimensional pump−probe, transient-2DIR, and the MD simulations.

Temperature Decay. The time-dependence of the one-dimensional UV−IR transient absorption line narrowing (Figure 3) provides a lower limit of 44 ± 17 ps for vibrational cooling. Our data are also in agreement with the results of Steinhurst et al.,[29] in that no anharmonic CO transitions are present after photodissociation, indicating that the excess energy is largely deposited into the low-frequency modes of the molecule. Although a general quantum mechanical treatment that rigorously describes the temperature dependence of absorption line shapes remains a challenge, the basic assumption is that the absorption width, caused by population of the low-frequency modes, is proportional to the nonequilibrium temperature of the molecules as it is described by our anharmonic model above. The measured orientational rates from transient-2DIR, which by Debye−Stokes−Einstein theory are proportional to temperature, should be a more accurate reporter of the molecular temperature. These values show a temperature relaxation of 70 ± 16 ps, which is a reasonable value given the large amount of evidence for weak system−solvent interactions in nonpolar solvents. It is a natural extension of the present work to consider solvents with varying polarity, polarizability, viscosity, and thermal conductivity to determine the relative importance of these parameters in promoting microscopic, nonequilibrium temperature relaxation. For the present study, the nonpolar solvent cyclohexane was chosen as it results in a particularly clearly resolved IR spectrum.

A photoproduct cooling rate is also obtained from the molecular dynamics simulations. Analysis of the photoproduct temperature decay yields a value of 8.01 ps, which is about an order of magnitude faster than experiment. The disparity with experiment is likely due to larger system−solvent interactions present in the MD simulations coupled with solvent molecular diffusion that was found to be roughly one-half the experimental value. Despite the numerical disparity, however, we measure the temperature of the instantaneous solvation shell and observe that it indeed remains near the equilibrium value. This fast energy dissipation away from the solvation shell can occur by either fast energy transfer among the molecules or by rapid exchange of solvent molecules between the solvation shell and the bulk solvent. To answer this question, we performed a similar nonequilibrium simulation, using identical MD parameters, except the temperature of a single solvent molecule was increased by adding kinetic energy (uniformly scaling all of the atom velocities). Monitoring the temperature relaxation back to the equilibrium value revealed a time constant of 5.3 ps, similar to that of the $Mn(CO)_5$ photoproducts. A solvent self-diffusion constant of $1.14 \pm 0.03 \times 10^{-5}$ cm^2/s is obtained from the velocity−velocity autocorrelation function. This value is smaller than the experimental value of 2.09×10^{-5} cm^2/s,[62] suggesting that the very fast heat transfer is not mediated by motional diffusion, but rather intermolecular energy transfer whose rate is overestimated by the simulation. A temperature decay time scale on the order of 5 ps is consistent with a simple comparison to the experimental thermal conductivity k_{th} of cyclohexane (0.123 W/m·K). The thermal conductance g_{th} is defined as the amount of heat transferred per second over a distance L across an area A for each degree difference of temperature:[63]

$$g_{th} = \frac{Ak_{th}\Delta T}{L} \tag{8}$$

Assuming a solute radius of 3 Å and length of 10 Å, it would take 5.9 ps for 148 kJ/mol of energy to transfer from a single cyclohexane molecule heated 300 K above its surroundings. Although the length is somewhat arbitrary, it is reasonable to assume that the transfer of energy 1 nm away from a solute is sufficiently dissipated. It would appear that the MD simulation captures the heat transfer of the pure solvent, but fails to adequately reproduce the heterogeneous heat transfer of the hot photoproduct to solution. In a classical system, the rate of vibrational energy relaxation is proportional to the force−force autocorrelation function of the solvent molecules onto a specific normal mode of the solute.[13] The fast rate of relaxation observed in our simulations likely arises from an overestimation of the solute−solvent interactions (friction, etc). Because force fields are generally calibrated under equilibrium conditions, the refinement of these force fields and their use under nonequilibrium conditions warrants further investigation.

Inhomogeneous Line Shapes. The inhomogeneous absorption line widths computed via vibrational perturbation theory (Figure 9) are approximately 20% of the experimental absorption width, and they are largely invariant with respect to temperature. From the peak-width fit (Figure 3), it is observed that the equilibrium absorption width of $Mn(CO)_5$ is 7.1 ± 0.8 cm^{-1}, a value that is larger than the 5.8 cm^{-1} width of the 2013 cm^{-1} peak of the parent. The experimental data were collected at 100 ps UV/IR delay, which means that the $Mn(CO)_5$ molecules are

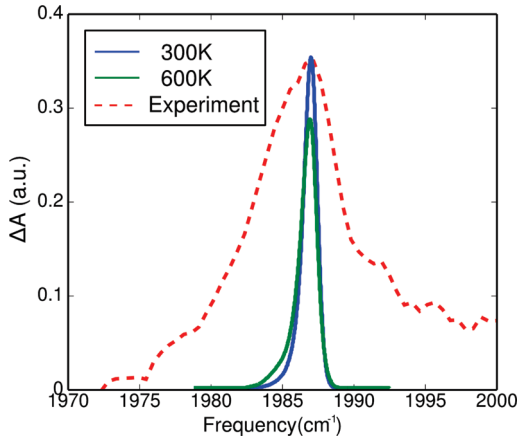

Figure 9. Computed inhomogeneous line shape of the $Mn(CO)_5$ carbonyl transition at 300 and 600 K using the anharmonic force constants given in the Supporting Information. The experimental UV/IR transient absorption at 100 ps time delay after subtraction of the overlapping bleach is shown in dashed lines for comparison. The center frequency of the simulated peaks was shifted to match the transient absorption frequency.

in thermal equilibrium with the solvent (~300 K), and so the broadness of the CO absorption is likely not due to temperature effects. This failure in reproducing the experimental width could arise from several origins: First, it may be possible that VPT2 does not accurately reproduce the coupling between the carbonyl and low-frequency modes of the molecule; because VPT2 successfully reproduces the anharmonic overtone shifts of the CO modes in $Mn_2(CO)_{10}$,[57] it is possible that this procedure underestimates the coupling to the low-frequency modes while overestimating the coupling among the CO modes. Second, given the radical nature of the molecule, it may be possible that interactions with the solvent distort the molecular geometry lifting the degeneracy of the two 1982 cm^{-1} carbonyl modes, thus giving an inherently broader line shape. Evidence for solvent complexation has been found in similar metal carbonyl radicals such as $W(CO)_5$ and $Cr(CO)_5$ from transient absorption measurements in *n*-hexane.[64] We anticipate improvements in experimental sensitivity and in modeling transient spectra will enable detailed comparisons with these explanations, especially if it becomes possible to directly observe spectral diffusion of an inhomogeneously broadened photoproduct.

Conclusions and Summary

In conclusion, 400 nm excitation of $Mn_2(CO)_{10}$ triggers the homolytic cleavage of the Mn−Mn bond, producing $Mn(CO)_5$ radicals in solution. The excess photon energy is dissipated into the low frequency modes of the molecules, causing a temperature increase, which in turn affects orientational diffusion rates of the photoproduct. These orientational rates serve as a molecular thermometer, which allow the extraction of a cooling rate for the transient species after photoreaction. While the MD simulations confirm some experimental results such as the orientational time scales, significant questions remain with respect to the simulated cooling rates. Anharmonic line width calculations show that temperature alone cannot account for the broad absorption line shape in $Mn(CO)_5$ and other effects may contribute to inhomogeneous broadening. It is also likely that this first-principles approach may require further testing and validation in systems whose dynamics are better understood.

This work presents an experimental and theoretical study of the temperature-dependent dynamics of transient species in solution, illustrating the capabilities of transient-2DIR spectroscopy as a powerful technique to provide dynamical information beyond one-dimensional transient absorption experiments. We have directly measured the orientational lifetime of a transient species as a function of waiting time after the photoreaction as well as the vibrational cooling rate and absorption line widths as a function of transient, effective temperature. Molecular dynamics simulations provided further insight into reorientational lifetimes and vibrational cooling from a molecular perspective and allowed the results to be directly compared to experiment. The orientational relaxation times obtained by experiment and simulation are consistent in relative magnitude, showing the dimetal parent to be slower than the monometal photoproduct. Despite this nearly quantitative agreement, the temperature relaxation time constant was found to be an order of magnitude faster in the simulation than was determined experimentally from the transient 2DIR signal decay. The temperature dependence of the absorption line widths was treated using an anharmonic model based on vibrational perturbation theory using ab initio-derived force constants. The lack of agreement between the spectral modeling results and experimental absorption width warrants further testing and validation of the perturbation approach in systems with well-characterized dynamics. Although 2DIR spectra include rich spectral and dynamical information, they alone cannot provide a molecular level picture. Classical MD simulations have been successful in helping to explain equilibrium 2DIR spectra, even those of the complex dynamics in liquid water. This work suggests, however, that the transient dynamics probed by nonequilibrium multidimensional methods pose a challenge to existing simulation methods.

In summary, we presented a unified ultrafast experimental and theoretical approach to understanding the nonequilibrium dynamics of $Mn(CO)_5$ following photodissociation. Future experimental work will elucidate the role of solvent polarity, polarizability, and viscosity in determining the temperature decay and orientational relaxation rates for both photoproducts of $Mn_2(CO)_{10}$.

Acknowledgment. We thank Prof. Eitan Geva and his research group for insightful discussions, and Prof. Barry Dunietz for providing access to computational resources. We gratefully acknowledge support from the National Science Foundation [CHE-0748501], the ACS Petroleum Research Fund [47048-G6], and an Excellence in Research Fellowship (C.R.B.).

Supporting Information Available: Density functional theory computation of inhomogeneous line shapes and fitting 2DIR peak volumes as a function of waiting time. This material is available free of charge via the Internet at http://pubs.acs.org.

References and Notes

(1) Cho, M. *Chem. Rev.* **2008**, *108*, 1331.
(2) Hamm, P.; Lim, M. H.; Hochstrasser, R. M. *J. Phys. Chem. B* **1998**, *102*, 6123.
(3) Bredenbeck, J.; Helbing, J.; Hamm, P. *J. Am. Chem. Soc.* **2004**, *126*, 990.
(4) Kolano, C.; Helbing, J.; Bucher, G.; Sander, W.; Hamm, P. *J. Phys. Chem. B* **2007**, *111*, 11297.
(5) Baiz, C.; Nee, M.; McCanne, R.; Kubarych, K. *Opt. Lett.* **2008**, *33*, 2533.
(6) Stewart, A. I.; Kania, R.; Greetham, G. M.; Clark, I. P.; Towrie, M.; Parker, A. W.; Hunt, N. T., submitted.
(7) Bakker, H. J.; Woutersen, S.; Nienhuys, H. K. *Chem. Phys.* **2000**, *258*, 233.
(8) Woutersen, S.; Bakker, H. J. *Nature* **1999**, *402*, 507.
(9) Anfinrud, P. A.; Han, C.; Hochstrasser, R. M. *Proc. Natl. Acad. Sci. U.S.A.* **1989**, *86*, 8387.

(10) Lim, M. H.; Jackson, T. A.; Anfinrud, P. A. *Nat. Struct. Biol.* **1997**, *4*, 209.
(11) Bredenbeck, J.; Helbing, J.; Nienhaus, K.; Nienhaus, G. U.; Hamm, P. *Proc. Natl. Acad. Sci. U.S.A.* **2007**, *104*, 14243.
(12) Harris, C. B.; Smith, D. E.; Russell, D. J. *Chem. Rev.* **1990**, *90*, 481.
(13) Chesnoy, J.; Gale, G. M. *Ann. Phys.* **1984**, *9*, 893.
(14) Adelman, S. A.; Stote, R. H. *J. Chem. Phys.* **1988**, *88*, 4397.
(15) Whitnell, R. M.; Wilson, K. R.; Hynes, J. T. *J. Chem. Phys.* **1992**, *96*, 5354.
(16) Whitnell, R. M.; Wilson, K. R.; Hynes, J. T. *J. Phys. Chem.* **1990**, *94*, 8625.
(17) Backus, E. H. G.; Nguyen, P. H.; Botan, V.; Pfister, R.; Moretto, A.; Crisma, M.; Toniolo, C.; Stock, G.; Hamm, P. *J. Phys. Chem. B* **2008**, *112*, 9091.
(18) Dougherty, T. P.; Grubbs, W. T.; Heilweil, E. J. *J. Phys. Chem.* **1994**, *98*, 9396.
(19) Herrick, R. S.; Brown, T. L. *Inorg. Chem.* **1984**, *23*, 4550.
(20) Hughey, J. L.; Anderson, C. P.; Meyer, T. J. *J. Organomet. Chem.* **1977**, *125*, C49.
(21) Kobayashi, T.; Ohtani, H.; Noda, H.; Teratani, S.; Yamazaki, H.; Yasufuku, K. *Organometallics* **1986**, *5*, 110.
(22) Lee, M.; Harris, C. B. *J. Am. Chem. Soc.* **1989**, *111*, 8963.
(23) Levenson, R. A.; Gray, H. B. *J. Am. Chem. Soc.* **1975**, *97*, 6042.
(24) Meyer, T. J.; Caspar, J. V. *Chem. Rev.* **1985**, *85*, 187.
(25) Owrutsky, J. C.; Baronavski, A. P. *J. Chem. Phys.* **1996**, *105*, 9864.
(26) Rosa, A.; Ricciardi, G.; Baerends, E. J.; Stufkens, D. J. *Inorg. Chem.* **1996**, *35*, 2886.
(27) Rothberg, L. J.; Cooper, N. J.; Peters, K. S.; Vaida, V. *J. Am. Chem. Soc.* **1982**, *104*, 3536.
(28) Seder, T. A.; Church, S. P.; Weitz, E. *J. Am. Chem. Soc.* **1986**, *108*, 7518.
(29) Steinhurst, D. A.; Baronavski, A. P.; Owrutsky, J. C. *Chem. Phys. Lett.* **2002**, *361*, 513.
(30) Waldman, A.; Ruhman, S.; Shaik, S.; Sastry, G. N. *Chem. Phys. Lett.* **1994**, *230*, 110.
(31) Zhang, J. Z.; Harris, C. B. *J. Chem. Phys.* **1991**, *95*, 4024.
(32) Dougherty, T. P.; Heilweil, E. J. *J. Chem. Phys.* **1994**, *100*, 4006.
(33) George, M. W.; Dougherty, T. P.; Heilweil, E. J. *J. Phys. Chem.* **1996**, *100*, 201.
(34) Wang, Z. H.; Pakoulev, A.; Dlott, D. D. *Science* **2002**, *296*, 2201.
(35) Deak, J. C.; Iwaki, L. K.; Dlott, D. D. *J. Phys. Chem. A* **1998**, *102*, 8193.
(36) Dlott, D. D. *Chem. Phys.* **2001**, *266*, 149.
(37) Tao, T. *Biopolymers* **1969**, *8*, 609.
(38) Berne, B.; Pecora, R. *Dynamic Light Scattering: With Applications to Chemistry, Biology, and Physics*; Dover Publications: Mineola, NY, 2000.
(39) Tokmakoff, A. *J. Chem. Phys.* **1996**, *105*, 1.
(40) Bredenbeck, J.; Helbing, J.; Hamm, P. *J. Chem. Phys.* **2004**, *121*, 5943.
(41) Tokmakoff, A. *J. Chem. Phys.* **1996**, *105*, 13.
(42) Baiz, C. R.; Nee, M. J.; McCanne, R.; Kubarych, K. J. *Opt. Lett.* **2008**, *33*, 2533.
(43) Tauber, M. J.; Mathies, R. A.; Chen, X. Y.; Bradforth, S. E. *Rev. Sci. Instrum.* **2003**, *74*, 4958.
(44) Nee, M. J.; McCanne, R.; Kubarych, K. J.; Joffre, M. *Opt. Lett.* **2007**, *32*, 713.
(45) Wang, J.; Wang, W.; Kollman, P. A.; Case, D. A. *J. Mol. Graphics Modell.* **2006**, *25*, 247.
(46) Wang, J.; Wolf, R. M.; Caldwell, J. W.; Kollman, P. A.; Case, D. A. *J. Comput. Chem.* **2004**, *25*, 1157.
(47) Bayly, C. I.; Cieplak, P.; Cornell, W. D.; Kollman, P. A. *J. Phys. Chem.* **1993**, *97*, 10269.
(48) Singh, U. C.; Kollman, P. A. *J. Comput. Chem.* **1984**, *5*, 129.
(49) Frisch, M. J.; Trucks, G. W.; Schlegel, H. B.; Scuseria, G. E.; Robb, M. A.; Cheeseman, J. R.; Montgomery, J. A., Jr.; Vreven, T.; Kudin, K. N.; Burant, J. C.; Millam, J. M.; Iyengar, S. S.; Tomasi, J.; Barone, V.; Mennucci, B.; Cossi, M.; Scalmani, G.; Rega, N.; Petersson, G. A.; Nakatsuji, H.; Hada, M.; Ehara, M.; Toyota, K.; Fukuda, R.; Hasegawa, J.; Ishida, M.; Nakajima, T.; Honda, Y.; Kitao, O.; Nakai, H.; Klene, M.; Li, X.; Knox, J. E.; Hratchian, H. P.; Cross, J. B.; Bakken, V.; Adamo, C.; Jaramillo, J.; Gomperts, R.; Stratmann, R. E.; Yazyev, O.; Austin, A. J.; Cammi, R.; Pomelli, C.; Ochterski, J. W.; Ayala, P. Y.; Morokuma, K.; Voth, G. A.; Salvador, P.; Dannenberg, J. J.; Zakrzewski, V. G.; Dapprich, S.; Daniels, A. D.; Strain, M. C.; Farkas, O.; Malick, D. K.; Rabuck, A. D.; Raghavachari, K.; Foresman, J. B.; Ortiz, J. V.; Cui, Q.; Baboul, A. G.; Clifford, S.; Cioslowski, J.; Stefanov, B. B.; Liu, G.; Liashenko, A.; Piskorz, P.; Komaromi, I.; Martin, R. L.; Fox, D. J.; Keith, T.; Al-Laham, M. A.; Peng, C. Y.; Nanayakkara, A.; Challacombe, M.; Gill, P. M. W.; Johnson, B.; Chen, W.; Wong, M. W.; Gonzalez, C.; Pople, J. A. *Gaussian 03*; Gaussian, Inc.: Wallingford, CT, 2004.
(50) Berendsen, H. J. C.; Postma, J. P. M.; van Gunsteren, W. F.; DiNola, A.; Haak, J. R. *J. Chem. Phys.* **1984**, *81*, 3684.
(51) Van Der Spoel, D.; Hess, E. L. B.; Groenhof, G.; Mark, A. E.; Berendsen, H. J. C. *J. Comput. Chem.* **2005**, *26*, 1701.
(52) Hamm, P.; Ohline, S. M.; Zinth, W. *J. Chem. Phys.* **1997**, *106*, 519.
(53) Schneider, W.; Thiel, W. *Chem. Phys. Lett.* **1989**, *157*, 367.
(54) Dressler, S.; Thiel, W. *Chem. Phys. Lett.* **1997**, *273*, 71.
(55) Barone, V. *J. Chem. Phys.* **2005**, *122*, 014108.
(56) Califano, S. *Vibrational States*; John Wiley and Sons: London, 1976.
(57) Baiz, C. R.; McRobbie, P. L.; Anna, J.; Geva, E.; Kubarych, K. J. *Acc. Chem. Res.*, in press.
(58) Nee, M.; Baiz, C.; Anna, J.; McCanne, R.; Kubarych, K. *J. Chem. Phys.* **2008**, *129*, 084503.
(59) Sando, G. M.; Zhong, Q.; Owrutsky, J. C. *J. Chem. Phys.* **2004**, *121*, 2158.
(60) Woutersen, S.; Emmerichs, U.; Nienhuys, H. K.; Bakker, H. J. *Phys. Rev. Lett.* **1998**, *81*, 1106.
(61) Moore, P.; Tokmakoff, A.; Keyes, T.; Fayer, M. D. *J. Chem. Phys.* **1995**, *103*, 3325.
(62) Sanni, S. A.; Fell, C. J. D.; Hutchinson, H. P. *J. Chem. Eng. Data* **1971**, *16*, 424.
(63) Berman, R. *Thermal Conduction in Solids*; Clarendon Press: Oxford, 1976.
(64) Dougherty, T. P.; Heilweil, E. J. *Chem. Phys. Lett.* **1994**, *227*, 19.

JP9027595